



# Auto-transition of vortex- to vector-Airy beams via liquid crystal q-Airy-plates

BINGYAN WEI,<sup>1,\*</sup> SHUXIA QI,<sup>1</sup> SHENG LIU,<sup>1</sup> PENG LI,<sup>1</sup> YI ZHANG,<sup>1</sup> LEI HAN,<sup>1</sup> JINZHAN ZHONG,<sup>1</sup> WEI HU,<sup>2</sup> YANQING LU,<sup>2</sup> AND JIANLIN ZHAO<sup>1,3</sup>

<sup>1</sup>MOE Key Laboratory of Material Physics and Chemistry under Extraordinary Conditions, and Shaanxi Key Laboratory of Optical Information Technology, School of Science, Northwestern Polytechnical University, Xi'an 710129, China

<sup>2</sup>National Laboratory of Solid State Microstructures, College of Engineering and Applied Sciences, and Collaborative Innovation Center of Advanced Microstructures, Nanjing University, Nanjing 210093, China

<sup>3</sup>jlzhao@nwpu.edu.cn

\*wbyxz@nwpu.edu.cn

**Abstract:** We propose the auto-transition of vortex-Airy to vector-Airy beams realized via a liquid crystal q-Airy-plate, whose director distribution is the integration of a q-plate and a polarization Airy mask. The polarization, phase, intensity distributions of the vortex-vector-Airy beams (VVABs) during the transition process and individual trajectories of the vortex beam, vector beam and Airy beam components are both theoretically and experimentally investigated. Interesting findings show that the pair of vortex components firstly experience transverse deflection with a smaller acceleration than the Airy components and then automatically evolve into a vector component propagating in a straight path. The polarization mode of the VVABs can be easily switched by tuning the incident polarization direction. Meanwhile, the Airy component still maintains its intrinsic self-accelerating and self-healing properties. The asymmetric intensity distribution and variation of VVABs are revealed, and the energy flows are simulated to better illustrate the interaction of the Airy, vortex and vector components. This work provides an approach for the manipulation of the spatially structured light beams, which may inspire their potential applications in optics, photonics and multidisciplinary fields.

© 2019 Optical Society of America under the terms of the [OSA Open Access Publishing Agreement](#)

## 1. Introduction

Spatially structured light beams [1] have attracted intensive research interest in recent years, among which the Airy beams, vortex beams and vector beams with spatially varying intensity, phase and polarization distributions accordingly are hot topics. Airy beams are a kind of nondiffracting beams [2] with self-healing [3] and transverse acceleration [4] properties, whose applications range from particles manipulation [5], light-sheet microscopy [6], generation of curved plasma channel [7] and spatiotemporal light bullets [8], to propagation against atmospheric turbulence [9]. Vortex beams and cylindrical vector beams are both in donut shapes featured by helical phase fronts [10] associated with orbital angular momentum (OAM) [11] and axis symmetry in polarization [12], respectively. Vortex beams with quantized OAM of  $\hbar$  [11] can be widely used in optical tweezers [13], stimulated-emission-depletion fluorescence microscopy [14], quantum informatics [15], vortex coronagraphs [16] and so on. As a typical cylindrical vector beam, radially polarized beam plays important roles in high-resolution imaging [17], optimal plasmonic focusing [18], metallic particles' trapping [19], laser processing [20], etc. Naturally, the Airy beams embedded with helical phase or axis symmetric polarization, known as vortex-Airy beams (VoABs) or vector-Airy beams (VeABs), may find special applications such as the abrupt polarization transitions and spin-orbit interactions [21].

Researches on two-dimensional (2D) VoABs or VeABs have been developing in recent years. Mazilu *et al.* were the first ones to propose the realization of VoABs to achieve the acceleration of vortex beams in Airy beams [22]. Dai *et al.* theoretically studied the propagation properties of VoABs [23] and then experimentally carried out their generations [24]. These generation strategies are mainly based on modulating the Gaussian beams via cubic or  $3/2$  phase patterns superimposed by phase singularities. Another way to obtain VoAB is illuminating the vortex beam generator with Airy beam produced by spatial light modulator or the cubic phase plate [25,26], and VeAB can also be acquired by tuning the polarization state of the incident Airy beam [27]. Deng *et al.* theoretically investigated the propagation of VoAB in uniaxial crystals [28], through slabs of right-/left-handed materials [29], and in a harmonic potential [30]. The reports on the propagation dynamics of VeABs are relatively limited, one of which is about their self-accelerating and self-healing features [31]. Despite all these works, few attentions have been paid to the combination or transition between VoABs and VeABs, which we propose as vortex-vector-Airy beams (VVABs). Therefore, studies on these more complicated spatially structured light beams possess fundamental significance.

In this paper, we present the auto-transition of 2D VoABs to VeABs accomplished by the liquid crystal (LC) q-Airy-plate [32], a Pancharatnam-Berry phase optical element [33] whose director distribution is the integration of a q-plate [34,35] and a polarization Airy mask [36]. The intensity, polarization and phase distributions of VVABs along propagation distances during the transition are both theoretically and experimentally investigated, and the trajectories of the Airy beam, vortex beam and vector beam components are analyzed, respectively. Moreover, the energy flows of the VVABs are simulated for better comprehension of their transition dynamics. This research offers a platform for the modulation of Airy beams decorated with vortex and vector beams, promoting their potential applications in multi-dimensional optical manipulation, higher-resolution biological observation and even some uncharted territories.

## 2. Theoretical analysis and experimental setup

As is mentioned above, the director distribution of a LC q-Airy-plate  $\alpha$  can be described as [37]

$$\alpha = q\varphi + (x^3 + y^3)/2, \quad (1)$$

where  $q$  equals half of the topological charge  $m$  of the corresponding vortex beam [38],  $\varphi(x, y) = \arctan(y/x)$  is the azimuthal angle, and  $(x^3 + y^3)$  is the cubic phase distribution. When we set the incident Gaussian beam to be linearly polarized (LP), its electric field can be expressed by

$$\mathbf{E}_{\text{in}} = E_0 \begin{bmatrix} \cos \theta \\ \sin \theta \end{bmatrix} = E_0 \left( \frac{e^{-i\theta}}{2} \begin{bmatrix} 1 \\ i \end{bmatrix} + \frac{e^{i\theta}}{2} \begin{bmatrix} 1 \\ -i \end{bmatrix} \right), \quad (2)$$

where  $\theta$  is the angle between the incident polarization direction and the  $x$  axis,  $[1, \pm i]^T$  is the Jones vector of left circularly polarized (LCP, +)/right circularly polarized (RCP, -) light [39]. After passing through the LC q-Airy-plate under the half-wave condition, the Gaussian beam will be transformed into

$$\begin{aligned} \mathbf{E}_{\text{out}} = \mathbf{M} \cdot \mathbf{E}_{\text{in}} &= E_0 \begin{bmatrix} \cos 2\alpha & \sin 2\alpha \\ \sin 2\alpha & -\cos 2\alpha \end{bmatrix} \left( \frac{e^{-i\theta}}{2} \begin{bmatrix} 1 \\ i \end{bmatrix} + \frac{e^{i\theta}}{2} \begin{bmatrix} 1 \\ -i \end{bmatrix} \right) \\ &= \frac{E_0}{2} \left( e^{i2q\varphi} e^{i(x^3+y^3)} e^{-i\theta} \begin{bmatrix} 1 \\ -i \end{bmatrix} + e^{-i2q\varphi} e^{-i(x^3+y^3)} e^{i\theta} \begin{bmatrix} 1 \\ i \end{bmatrix} \right), \end{aligned} \quad (3)$$

where  $\mathbf{M}$  is the Jones matrix of the q-Airy-plate. From Eq. (3) we can see that, the output light field consists of two parts: RCP and LCP components, and they both exhibit the helical

phase front  $\exp(i|2q\varphi|)$  and the cubic phase modulation  $\exp(i|x^3+y^3|)$  (that is, RCP and LCP VoABs). The different signs of the helical and cubic phase factors indicate that the spiral wave fronts of the vortex beam components twist and the modulated Airy beam components automatically move in opposite directions. With the increase of the propagation distance, the superimposition of RCP and LCP vortex components with opposite topological charges can eventually result in the existence of vector beam [40], implementing the auto-transition from phase singularities to polarization singularity. And the polarization mode of the vector part depends on the parameter  $\theta$ . As the phase singularities still exist before the vector component fully takes place, we uniformly define the combined singular beams in intermediate states as vortex-vector beams [41]. Considering the Airy beam element, the auto-transition between the VoABs and VeABs or the generation of VVABs of different types can thus be achieved.

To characterize the transition dynamics of the VVABs modulated through the LC q-Airy-plate, we adopt an optical setup illustrated in Fig. 1. A He-Ne laser with wavelength of 632.8 nm is utilized as the Gaussian light source. A polarizer and a  $\lambda/2$  plate are set in sequence to control the incident beam to be linearly polarized at different  $\theta$ . To implement the Fourier transformation, a spherical lens is placed 125 mm (focal length) away from the LC q-Airy-plate. A CCD is set at the focal plane of the lens at first, which is defined as the initial observation point (propagation distance  $d = 0$ ). Another polarizer is selectively inserted between the lens and the CCD to analyze the output polarization. Herein, for simplicity, we take the q(0.5)-Airy-plate to study the propagation dynamics of the modulated VVABs. The nematic LC q-Airy-plates are fabricated via the sulfonic azo-dye material SD1 based photoalignment technique and the digital micro-mirror device based micro-lithography system [42]. The micrograph and director distribution of the q(0.5)-Airy-plate in the inset of Fig. 1 indicate the LC directors vary periodically and continuously, composing the space-variant cubic pattern inserted with a spiral structure. High optical efficiency of over 90% is achieved by applying proper voltage to keep the sample under the half-wave condition. For LC q-Airy-plates with larger  $q$  values, the theoretical simulation and experimental analysis concluded in this work are applicable as well.

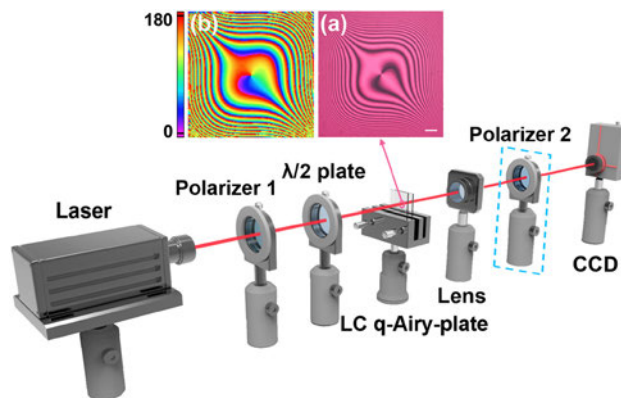


**Fig. 1.** Experimental setup for characterizing the transition from VoABs to VeABs. (a) Micrograph and (b) detected director distribution of the LC q(0.5)-Airy-plate. The scale bar is 100  $\mu\text{m}$ . The color bar indicates the LC director varying from  $0^\circ$  to  $180^\circ$ .

### 3. Results and discussions

Firstly, the polarization states of the modulated beams are investigated. Figure 2 shows the detected intensity distributions analyzed by Polarizer 2 at  $d = 0$  under the horizontally ( $\theta = 0^\circ$ ) and vertically ( $\theta = 90^\circ$ ) LP illumination, respectively. From Figs. 2(a)–2(d) we can see that,

with the rotation of Polarizer 2, the transmitted main lobes in the central parts also vary, and their connections are parallel with the directions of Polarizer 2, revealing the polarization pattern features of a radially polarized beam. While for Figs. 2(e)–2(h), the lobed patterns are perpendicular to the directions of Polarizer 2, exhibiting the features of an azimuthally polarized beam. The slightly “s”-shaped patterns verify the characteristic of vortex-vector beam [43], which also indicates the light fields of the dual VoABs have already interacted to be VVABs. The 0th order Gaussian beam at the center results from the residual phase of the LC sample [44]. The side beamlets are mainly circular polarized, thus their intensities remain unchanged.

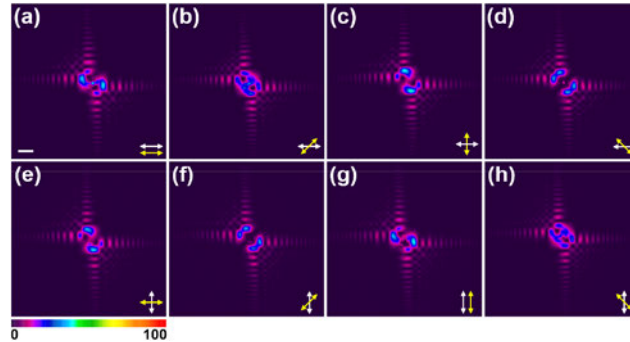


**Fig. 2.** Intensity distributions of the (a)–(d) radial and (e)–(h) azimuthal VVABs analyzed by Polarizer 2. The directions of the incident polarization and Polarizer 2 are marked by white and yellow arrows, respectively. The scale bar is 500  $\mu\text{m}$ .

In order to study the polarization properties of the VVABs when propagating, a digital holographic imaging system [45] and the Stokes method [46,47] are employed. Figures 3(d)–3(f) and 3(j)–3(l) are detected polarization distributions of the radial and azimuthal VVABs at  $d = 0, 30, 100$  cm, respectively, with LCP and RCP states marked by blue and red ellipses. Corresponding intensity distributions, which are similar to the symmetric Airy beams [48,49], are shown in the background. The experiment results are consistent with the simulations in Figs. 3(a)–3(c) and 3(g)–3(i) except for some measurement errors. These images vividly show that as the RCP and LCP VoABs move towards each other, the overlap and interaction of their light fields lead to more and more spatially LP components. After the entire superimposition of the vortex beam components, the radial or azimuthal polarization distribution of vector beam is constructed, with some circular and elliptical polarizations distributed at the recovered Airy beams. Thus, the final light fields can be regarded as VeABs of radial and azimuthal modes, respectively. More generalized VVABs can also be easily acquired by adjusting the incident  $\theta$ , providing flexibility for laser processing.

Furthermore, researches on the transverse deflection of VVABs are conducted. Figure 4(a) depicts the trajectories of the Airy, vortex and vector components, in which the red circles, blue crosses and magenta asterisks are experimental deflection results of the Airy, vortex and vector components, respectively, the red and blue lines are the parabolic fit of the Airy and the vortex components correspondingly, and the magenta line is the linear fit of the vector component. Herein, the deflection of the Airy component is defined as the lateral displacement of the center of mass, while the deflection of the vortex or vector component refers to the displacement of the center of the dark core compared to their original positions at  $d = 0$  cm. These curves manifest that influenced by the Airy component's self-accelerating propagation, the vortex component also experiences transverse deflections at first. With the increase of  $d$ , the dark core of the vortex component is gradually covered by the reconstructed main lobe of the Airy component, which can be reflected by the transverse profiles at  $d = 10, 30, 50$  cm inserted in Fig. 4(a). Therefore, the

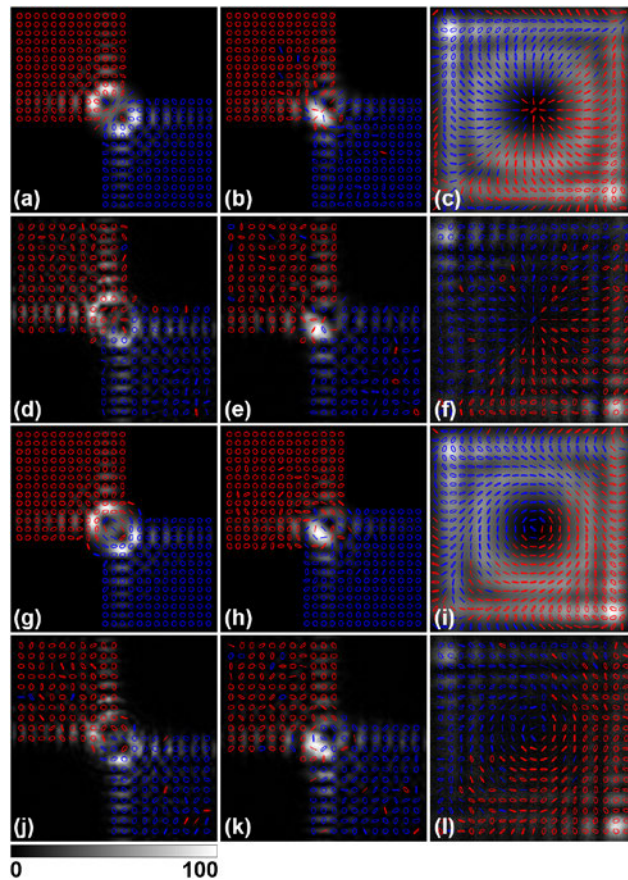


**Fig. 3.** (a)-(c)/(g)-(i) Simulated and (d)-(f)/(j)-(l) experimental polarization distributions of radial/azimuthal VVAB at  $d = 0, 30, 100$  cm. Blue and red ellipses represent the left-handed and right-handed polarization, respectively.

trajectory of vortex component between 20 cm to 50 cm can be hardly identified. Afterwards, the dark core of the vector component reappears in the center of the VVAB and travels in a straight path. These experiment results are in agreement with the simulated side view propagation of the  $m = 1$  VVAB shown in Fig. 4(b). Besides, the side view of the  $m = 2$  VVAB (Fig. 4(c)), whose simulated and experimental intensity distributions are shown in Figs. 4(d) and 4(e) respectively, is also presented for comparison. From these images we can see that although the distortion of the main lobe becomes larger due to the introduction of the double helix wave front, the deflection keeps the same with that of the  $m = 1$  VVAB (e.g., the lateral displacements are both 1.5 mm at  $d = 100$  cm), validating the applicability of the analyses based on  $m = 1$  VVAB.

In addition, through in-depth analysis of Fig. 4(b), it can be found that the parabolic curvature of the vortex component is slightly smaller than that of the Airy component. To give a more detailed comparison, we further detect the phase distributions of the VVAB based on digital holography [45]. As shown in the inset of Fig. 5, the clear phase distributions detected at different  $d$  allow us to identify the exact positions of the phase singularities (marked by black circles), whose lateral displacement can also be regarded as the deflection of the vortex component. By measuring the movement of the phase singularities, more accurate trajectory of the vortex component is plotted in Fig. 5. Comparing the two curves we can find that the deflection of the Airy component is larger than that of the vortex component at the same propagation

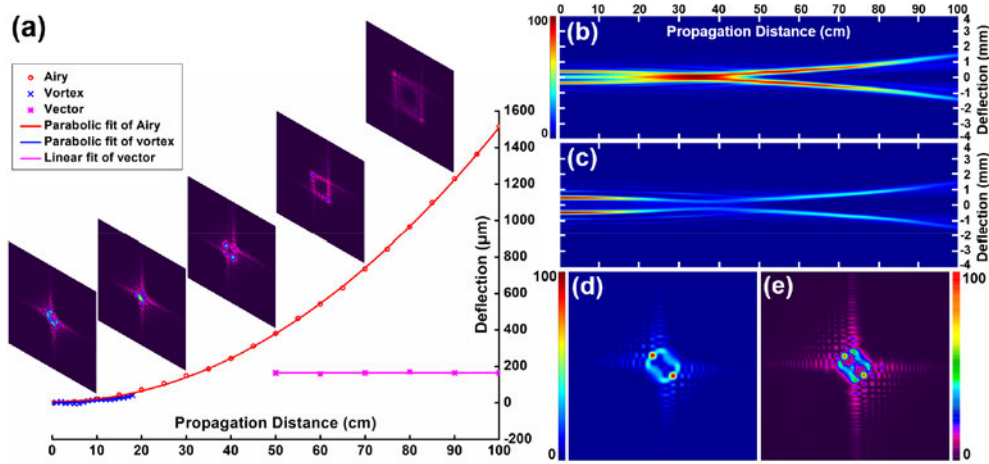


**Fig. 4.** (a) Trajectories of the Airy, vortex and vector components with some intensity distributions inserted at corresponding distances. Simulated side view propagation of (b)  $m = 1$  and (c)  $m = 2$  VVABs. (d) Simulated and (e) experimental intensity distribution of  $m = 2$  VVAB at  $d = 0$  cm.

distance, verifying that the vortex component propagates with a slower acceleration. Note that although the accelerating propagation of the vortex beam imposed on an Airy beam has been analyzed theoretically [23], the result we obtain differs from previous conclusions that the vortex component accelerates with twice the velocity of the Airy component. This phenomenon is mainly caused by the initial locations of the vortex components at the main lobes of the Airy components herein, in which case there hasn't been an explicit formula that can describe the accurate trajectories of the vortex components. However, the reason for the different deflections between the Airy and vortex components can be deduced from the energy flow of the VVAB in the following analyses. As the deviation of the experiment results of the phase singularity from the parabolic fit is relatively large, to be more rigorous, we define the trajectory of the vortex beam as quasi-parabolic curve. Continuous phase dynamics of the VVAB from  $d = 0$  to  $d = 100$  cm is simulated in [Visualization 1](#), which also reveals that the phase singularities will firstly experience a small lateral displacement and then be distorted by the cubic phase. The spiral phases will ultimately merge into one with a  $\pi$  phase step, evincing the annihilation of vortex components and the generation of a vector component. This fancy dynamics of helical phases may find special applications in OAM based entanglement and quantum informatics [11].

It is worth mentioning that the captured transverse profiles of VVAB inserted in Fig. 4 exhibit the asymmetric variation of vortex component along  $-45^\circ/135^\circ$  relative to the transverse plane. To explain this phenomenon, we analyze the energy flow of the VVAB, whose Poynting vector  $\mathbf{S}$  can be described as [50]

$$\mathbf{S} = \frac{c^2 \varepsilon_0}{2\omega} \left\{ \text{Im}[\mathbf{E}^* \cdot (\nabla)\mathbf{E}] + \frac{1}{2} \nabla \times \text{Im}(\mathbf{E}^* \times \mathbf{E}) \right\}, \quad (4)$$

where  $c$  is the speed of light in vacuum,  $\varepsilon_0$  is the permittivity of free space,  $\omega$  is the angular frequency, and  $\mathbf{E}$  is the electric field of the VVAB expressed by Eq. (3). Figure 6 displays the simulated Poynting vector distributions at  $d = 0, 10, 20, 40, 60, 100$  cm, respectively. These images indicate that, on the one hand, the overall energy of the VVAB flows towards  $-45^\circ/135^\circ$  direction due to the intrinsic transverse acceleration property of Airy beam components. On the other hand, affected by the twisted wave fronts, the Poynting vector near the phase singularities rotates counterclockwise around the positive vortex component and clockwise around the negative

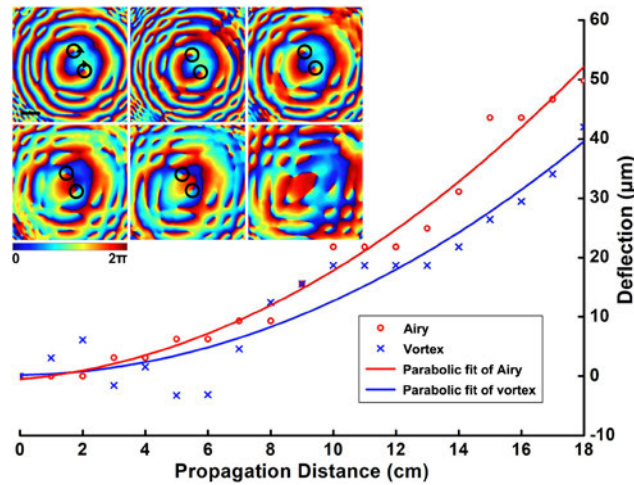


**Fig. 5.** Detailed transverse acceleration of the Airy and vortex components. The inserted phase distributions from the upper left to the lower right are detected at  $d = 0, 4, 8, 12, 16, 20$  cm, respectively. The phase singularities are marked by the black circles and the arrows denote the twist directions of the  $m = +1$  and  $m = -1$  vortex components. The scale bar is  $300 \mu\text{m}$ .

vortex component. Therefore, the intensity distribution around the vortex component is more concentrated on the right of the motion of the  $m = +1$  VoAB and left of the  $m = -1$  VoAB. This influence will take over until the Airy component reforms and the vector component appears. The reveal of asymmetric light field during propagation is crucial as it can be adopted to control the optical force when utilized as 3D optical tweezers. Additionally, the quasi-self-acceleration of vortex components can also be deduced from the energy flow. Figures 6(a)–6(c) suggest that affected by the energy flow of the Airy component, the Poynting vector of the vortex component deviates to  $-45^\circ$  or  $135^\circ$  direction, leading to the movement of the vortex component along with the Airy component. However, the intrinsic rotating energy flow of the vortex component weakens the diagonal acceleration. As a result, the vortex components propagate along a quasi-parabolic trajectory with a smaller acceleration velocity than the Airy components.

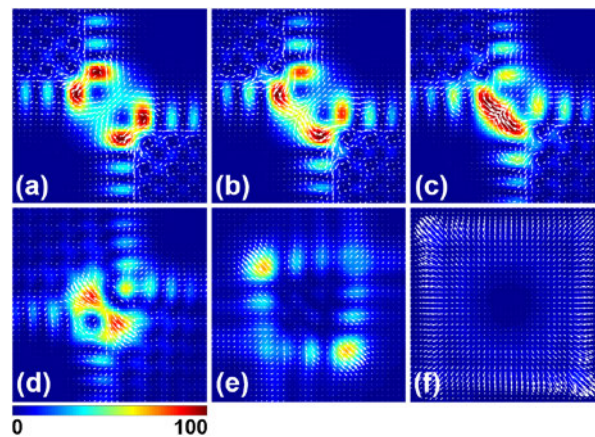


**Fig. 6.** (a)–(f) Simulated energy flows of the VVAB at  $d = 0, 10, 20, 40, 60, 100$  cm, with corresponding intensity distributions depicted in the background.

#### 4. Conclusion

In summary, we have demonstrated the auto-transition of 2D VoABs to VeABs realized via LC q-Airy-plates, and revealed the propagation dynamics of VVABs both theoretically and experimentally. By analyzing their polarization, phase and intensity distributions along propagation distances, we show that the VVABs are the product of the superimposition of RCP and LCP VoABs of opposite topological charges, and different modes can be realized by tuning the incident polarization direction. The trajectories indicate the Airy beam component still maintains its self-accelerating property, while the vortex beam components firstly experience transverse deflection with a smaller acceleration and then automatically evolve into a vector beam component propagating in a straight path. Affected by the helical wave front of the vortex component, the surrounding Poynting vector rotates during the self-healing process of the Airy component, leading to the asymmetric intensity distribution before the main lobe recovers. This study offers deep insight into the transition dynamics of the VoABs to VeABs and the intermediate VVABs modulated through the LC q-Airy-plates, promoting their further applications in optics and photonics, atmospheric science, biology, and even in some uncharted territories.

#### Funding

National Key R&D Program of China (2017YFA0303800); National Natural Science Foundation of China (NSFC) (11634010, 11774289, 11804277, 61675168, 91850118, U1630125); Fundamental Research Funds for the Central Universities (3102017OQD103, 3102019JC008); Open Foundation Project of National Laboratory of Solid State Microstructures (M31040).

#### References

1. N. M. Litchinitser, "Structured light meets structured matter," *Science* **337**(6098), 1054–1055 (2012).
2. G. A. Siviloglou, J. Broky, A. Dogariu, and D. N. Christodoulides, "Observation of accelerating Airy beams," *Phys. Rev. Lett.* **99**(21), 213901 (2007).
3. J. Broky, G. A. Siviloglou, A. Dogariu, and D. N. Christodoulides, "Self-healing properties of optical Airy beams," *Opt. Express* **16**(17), 12880–12891 (2008).
4. G. A. Siviloglou, J. Broky, A. Dogariu, and D. N. Christodoulides, "Ballistic dynamics of Airy beams," *Opt. Lett.* **33**(3), 207–209 (2008).
5. J. Baumgartl, M. Mazilu, and K. Dholakia, "Optically mediated particle clearing using Airy wavepackets," *Nat. Photonics* **2**(11), 675–678 (2008).
6. T. Vettenburg, H. I. C. Dalgarno, J. Nylk, C. Coll-Lladó, D. E. K. Ferrier, T. Čížmár, F. J. Gunn-Moore, and K. Dholakia, "Light-sheet microscopy using an Airy beam," *Nat. Methods* **11**(5), 541–544 (2014).
7. P. Polynkin, M. Kolesik, J. V. Moloney, G. A. Siviloglou, and D. N. Christodoulides, "Curved plasma channel generation using ultraintense Airy beams," *Science* **324**(5924), 229–232 (2009).
8. A. Chong, W. H. Renninger, D. N. Christodoulides, and F. W. Wise, "Airy-Bessel wave packets as versatile linear light bullets," *Nat. Photonics* **4**(2), 103–106 (2010).
9. Y. Gu and G. Gbur, "Scintillation of Airy beam arrays in atmospheric turbulence," *Opt. Lett.* **35**(20), 3456–3458 (2010).
10. A. M. Yao and M. J. Padgett, "Orbital angular momentum: origins, behavior and applications," *Adv. Opt. Photonics* **3**(2), 161–204 (2011).
11. S. Franke-Arnold, L. Allen, and M. Padgett, "Advances in optical angular momentum," *Laser Photonics Rev.* **2**(4), 299–313 (2008).
12. Q. Zhan, "Cylindrical vector beams: from mathematical concepts to applications," *Adv. Opt. Photonics* **1**(1), 1–57 (2009).
13. L. Paterson, M. P. MacDonald, J. Arlt, W. Sibbett, P. E. Bryant, and K. Dholakia, "Controlled rotation of optically trapped microscopic particles," *Science* **292**(5518), 912–914 (2001).
14. S. W. Hell and J. Wichmann, "Breaking the diffraction resolution limit by stimulated emission: stimulated-emission-depletion fluorescence microscopy," *Opt. Lett.* **19**(11), 780–782 (1994).
15. G. Molina-Terriza, J. P. Torres, and L. Torner, "Twisted photons," *Nat. Phys.* **3**(5), 305–310 (2007).
16. J. H. Lee, G. Foo, E. G. Johnson, and G. A. Swartzlander, "Experimental verification of an optical vortex coronagraph," *Phys. Rev. Lett.* **97**(5), 053901 (2006).
17. X. Xie, Y. Chen, K. Yang, and J. Zhou, "Harnessing the point-spread function for high-resolution far-field optical microscopy," *Phys. Rev. Lett.* **113**(26), 263901 (2014).

18. W. Chen, D. C. Abeyasinghe, R. L. Nelson, and Q. Zhan, "Plasmonic lens made of multiple concentric metallic rings under radially polarized illumination," *Nano Lett.* **9**(12), 4320–4325 (2009).
19. C. Min, Z. Shen, J. Shen, Y. Zhang, H. Fang, G. Yuan, L. Du, S. Zhu, T. Lei, and X. Yuan, "Focused plasmonic trapping of metallic particles," *Nat. Commun.* **4**(1), 2891 (2013).
20. O. J. Allegre, W. Perrie, S. P. Edwardson, G. Dearden, and K. G. Watkins, "Laser microprocessing of steel with radially and azimuthally polarized femtosecond vortex pulses," *J. Opt.* **14**(8), 085601 (2012).
21. S. Liu, M. Wang, P. Li, P. Zhang, and J. Zhao, "Abrupt polarization transition of vector autofocusing Airy beams," *Opt. Lett.* **38**(14), 2416–2418 (2013).
22. M. Mazilu, J. Baumgartl, T. Čížmár, and K. Dholakia, "Accelerating vortices in Airy beams," *Proc. SPIE* **7430**, 74300C (2009).
23. H. T. Dai, Y. J. Liu, D. Luo, and X. W. Sun, "Propagation dynamics of an optical vortex imposed on an Airy beam," *Opt. Lett.* **35**(23), 4075–4077 (2010).
24. H. T. Dai, Y. J. Liu, D. Luo, and X. W. Sun, "Propagation properties of an optical vortex carried by an Airy beam: experimental implementation," *Opt. Lett.* **36**(9), 1617–1619 (2011).
25. Z. Cai, Y. Liu, C. Zhang, J. Xu, S. Ji, J. Ni, J. Li, Y. Hu, D. Wu, and J. Chu, "Continuous cubic phase microplates for generating high-quality Airy beams with strong deflection," *Opt. Lett.* **42**(13), 2483–2486 (2017).
26. Z. Cai, Y. Liu, Y. Hu, C. Zhang, J. Xu, S. Ji, J. Ni, Z. Lao, J. Li, Y. Zhao, D. Wu, and J. Chu, "Generation of colorful Airy beams and Airy imaging of letters via two-photon processed cubic phase plates," *Opt. Lett.* **43**(5), 1151–1154 (2018).
27. J. Zhou, Y. Liu, Y. Ke, H. Luo, and S. Wen, "Generation of Airy vortex and Airy vector beams based on the modulation of dynamic and geometric phases," *Opt. Lett.* **40**(13), 3193–3196 (2015).
28. D. Deng, C. Chen, X. Zhao, and H. Li, "Propagation of an Airy vortex beam in uniaxial crystals," *Appl. Phys. B: Lasers Opt.* **110**(3), 433–436 (2013).
29. B. Chen, C. Chen, X. Peng, and D. Deng, "Propagation of Airy Gaussian vortex beams through slabs of right-handed materials and left-handed materials," *J. Opt. Soc. Am. B* **32**(1), 173–178 (2015).
30. Z. Pang and D. Deng, "Propagation properties and radiation forces of the Airy Gaussian vortex beams in a harmonic potential," *Opt. Express* **25**(12), 13635–13647 (2017).
31. J. Bar-David, N. Voloch-Bloch, N. Mazurski, and U. Levy, "Unveiling the propagation dynamics of self-accelerating vector beams," *Sci. Rep.* **6**(1), 34272 (2016).
32. B. Y. Wei, P. Chen, S. J. Ge, W. Duan, W. Hu, and Y. Q. Lu, "Generation of self-healing and transverse accelerating optical vortices," *Appl. Phys. Lett.* **109**(12), 121105 (2016).
33. T. Zhan, J. Xiong, Y. H. Lee, and S. T. Wu, "Polarization-independent Pancharatnam-Berry phase lens system," *Opt. Express* **26**(26), 35026–35033 (2018).
34. W. Ji, C. H. Lee, P. Chen, W. Hu, Y. Ming, L. Zhang, T. H. Lin, V. Chigrinov, and Y. Q. Lu, "Meta-q-plate for complex beam shaping," *Sci. Rep.* **6**(1), 25528 (2016).
35. P. Chen, L. L. Ma, W. Duan, J. Chen, S. J. Ge, Z. H. Zhu, M. J. Tang, R. Xu, W. Gao, T. Li, W. Hu, and Y. Q. Lu, "Digitalizing self-assembled chiral superstructures for optical vortex processing," *Adv. Mater.* **30**(10), 1705865 (2018).
36. B. Y. Wei, P. Chen, W. Hu, W. Ji, L. Y. Zheng, S. J. Ge, Y. Ming, V. Chigrinov, and Y. Q. Lu, "Polarization-controllable Airy beams generated via a photoaligned director-variant liquid crystal mask," *Sci. Rep.* **5**(1), 17484 (2015).
37. B. Y. Wei, S. Liu, P. Chen, S. X. Qi, Y. Zhang, W. Hu, Y. Q. Lu, and J. L. Zhao, "Vortex Airy beams directly generated via liquid crystal q-Airy-plates," *Appl. Phys. Lett.* **112**(12), 121101 (2018).
38. L. Marrucci, C. Manzo, and D. Paparo, "Optical spin-to-orbital angular momentum conversion in inhomogeneous anisotropic media," *Phys. Rev. Lett.* **96**(16), 163905 (2006).
39. S. Liu, P. Li, Y. Zhang, X. Gan, M. Wang, and J. Zhao, "Longitudinal spin separation of light and its performance in three-dimensionally controllable spin-dependent focal shift," *Sci. Rep.* **6**(1), 20774 (2016).
40. S. Liu, S. Qi, Y. Zhang, P. Li, D. Wu, L. Han, and J. Zhao, "Highly efficient generation of arbitrary vector beams with tunable polarization, phase, and amplitude," *Photonics Res.* **6**(4), 228–233 (2018).
41. Y. S. Rumala, G. Milione, T. A. Nguyen, S. Pratavieira, Z. Hossain, D. Nolan, S. Slussarenko, E. Karimi, L. Marrucci, and R. R. Alfano, "Tunable supercontinuum light vector vortex beam generator using a q-plate," *Opt. Lett.* **38**(23), 5083–5086 (2013).
42. B. Y. Wei, W. Hu, Y. Ming, F. Xu, S. Rubin, J. G. Wang, V. Chigrinov, and Y. Q. Lu, "Generating switchable and reconfigurable optical vortices via photopatterning of liquid crystals," *Adv. Mater.* **26**(10), 1590–1595 (2014).
43. Z. Liu, Y. Liu, Y. Ke, Y. Liu, W. Shu, H. Luo, and S. Wen, "Generation of arbitrary vector vortex beams on hybrid-order Poincaré sphere," *Photonics Res.* **5**(1), 15–21 (2017).
44. X. W. Lin, W. Hu, X. K. Hu, X. Liang, Y. Chen, H. Q. Cui, G. Zhu, J. N. Li, V. Chigrinov, and Y. Q. Lu, "Fast response dual-frequency liquid crystal switch with photo-patterned alignments," *Opt. Lett.* **37**(17), 3627–3629 (2012).
45. S. Liu, L. Han, P. Li, Y. Zhang, H. Chengs, and J. Zhao, "A method for simultaneously measuring polarization and phase of arbitrarily polarized beams based on Pancharatnam-Berry phase," *Appl. Phys. Lett.* **110**(17), 171112 (2017).
46. P. Li, Y. Zhang, S. Liu, C. Ma, L. Han, H. Cheng, and J. Zhao, "Generation of perfect vectorial vortex beams," *Opt. Lett.* **41**(10), 2205–2208 (2016).
47. P. Li, D. Wu, Y. Zhang, S. Liu, Y. Li, S. Qi, and J. Zhao, "Polarization oscillating beams constructed by copropagating optical frozen waves," *Photonics Res.* **6**(7), 756–761 (2018).

48. Z. X. Fang, Y. Chen, Y. X. Ren, L. Gong, R. D. Lu, A. Q. Zhang, H. Z. Zhao, and P. Wang, "Interplay between topological phase and self-acceleration in a vortex symmetric Airy beam," *Opt. Express* **26**(6), 7324–7335 (2018).
49. P. Vaveliuk, A. Lencina, J. A. Rodrigo, and O. M. Matos, "Symmetric Airy beams," *Opt. Lett.* **39**(8), 2370–2373 (2014).
50. M. V. Berry, "Optical currents," *J. Opt. A: Pure Appl. Opt.* **11**(9), 094001 (2009).